The International Journal of Advanced Manufacturing Technology (2022) 120:6693–6705
https://doi.org/10.1007/s00170-022-09135-x

ORIGINAL ARTICLE

The prediction model and experimental research of grinding surface roughness based on AE signal

Guoqiang Yin[1] · Jiahui Wang[1] · Yunyun Guan[1] · Dong Wang[2] · Yao Sun[1]

Received: 13 January 2022 / Accepted: 24 March 2022 / Published online: 16 April 2022
© The Author(s), under exclusive licence to Springer-Verlag London Ltd., part of Springer Nature 2022

Abstract
This paper is based on the investigation of the relationship between the processing parameters and the characteristic parameters of acoustic emission signal (AE signal) including RMS value, ringing count, and signal spectrum during the grinding of several difficult-to-machine metallic materials; the variation of AE signal characteristic parameters and spectrum with the parameters of grinding depth a_p, grinding wheel velocity v_s, and feed velocity v_w was analyzed, then the corresponding relationship between acoustic emission signal characteristic parameters and machining surface roughness was given. On this basis, the multi-information fusion algorithm based on BP neural network was used to reasonably fuse various characteristic parameters of AE signals, then predict and recognize the surface roughness of grinding workpieces. Finally, the established model was optimized by using genetic algorithm, which significantly improved the prediction accuracy and provided a reliable prediction model for the grinding of difficult-to-machine alloys, providing a feasible method for predicting surface roughness for practical production.

Keywords AE signal · Multi-information fusion model · Grinding process · Surface roughness

1 Introduction

Grinding is a technique used in contemporary machining to achieve great surface precision while minimizing surface damage [1, 2]. However, grinding difficult-to-machine alloy materials is an extremely complicated process, the surface roughness of the material is not easy to control, and the surface roughness is sometimes large or small, and sometimes even may occur grinding burns and micro-cracks [3]. Therefore, it is of great urgence for developing a method that can accurately predict the grinding surface roughness of the workpiece and improve the performance of the processed parts. At the same time, the grinding process has been developing in the direction of automation and intelligence, and it is an effective way to analyze and judge the grinding process by using artificial neural network by collecting a large amount of state information in the grinding process through sensors [4, 5]. As a mature non-destructive monitoring method, acoustic emission technology is effectively used in grinding monitoring because of high sensitivity and strong anti-interference ability. In addition, the acoustic emission signal (AE signal) contains a wealth of information about the grinding process, and the time and frequency domain structure of the signal are very closely related to the contact condition of the grinding wheel and the workpiece, the surface quality of the workpiece, and the wear state of the grinding wheel, etc. Therefore, it is feasible to use the AE signal to monitor the grinding process, and satisfactory results have been achieved [6, 7].

In order to improve the intelligence level of grinding monitoring, scholars at home and abroad have conducted a lot of research on the principles and methods of multi-information fusion, which shows that multi-information fusion technology has a broad application prospect in grinding process monitoring. Ding et al. [8] proposed a surface roughness prediction model to introduce the relationship between surface roughness and the wear condition of grinding wheel grinding parameters. AE sensors were used to collect grinding signals during the grinding process to obtain the wear condition of

✉ Guoqiang Yin
yinguoqiang@me.neu.edu.cn

1 School of Mechanical Engineering and Automation, Northeastern University, Shenyang 110819, People's Republic of China

2 Shenyang National Laboratory for Materials Science, Institute of Metal Research, Chinese Academy of Sciences, Shenyang 110016, People's Republic of China

the grinding wheel. In addition, a fuzzy neural network is used to obtain the predicted surface roughness. And the prediction system is proved to be feasible with high prediction accuracy by experiments. Pandiyan et al. [9] monitored the abrasive belt grinding process using acceleration sensors, acoustic emission sensors, and force sensors, and extracted time and frequency domain features from the signals collected by the sensors, and optimized them using a genetic algorithm to obtain a subset with fewer input features. Arun et al. [10] established an experimental setup consisting of a piezoelectric acoustic emission sensor, a cylindrical grinding machine, and associated signal processing software and hardware, and extracted the root mean square value, amplitude, ring count, and average signal level characteristics of the acoustic emission signal from the collected acoustic emission signal time domain waveforms, and compared and correlated them with the surface roughness of the workpiece after grinding. Machine learning techniques such as decision trees, artificial neural networks, and support vector machines were used to predict the dull state of the grinding wheel. The results showed that the characteristic quantities of acoustic emission signals were strongly correlated with the surface roughness of the workpiece after grinding. Liu et al. [11] used the AE signal monitoring process in the polishing of sapphire wafers, determined experimentally that the RMS value of the AE signal is closely related with the material removal rate under various polishing conditions which are closely related, and developed a mathematical model to predict the processing results based on the experiments, and the prediction errors were all less than 12%. The analysis showed that the AE signal can be used as a parameter of the prediction model in the polishing process. Hweju et al. [12] investigated the correlation between AE signal parameters and surface roughness. The AE signal parameters were used to predict the surface roughness and three different models were established for comparison. On the basis of the mean absolute percentage error of the models, degree of correlation between the AE signal parameters on the accuracy of surface roughness prediction was measured. The degree of correlation between some processing parameters and surface roughness is then given.

In summary, this work analyzes the impact of grinding settings on several characteristic parameters of AE signal during the grinding of difficult-to-machine alloys to describe the relationship between each characteristic parameter of AE signal and surface roughness. Then, using the grinding experimental data to train a BP neural network, the BP neural network was used to the grinding surface roughness prediction process to provide a multi-information fusion prediction model of grinding surface roughness. To increase the model's prediction accuracy, it was improved using a genetic algorithm, and the model's prediction and recognition impacts were confirmed by trials, resulting in a prediction and auxiliary monitoring technique for real production.

2 Building of BP neural network

The BP neural network has two processes during the training process: forward transmission of signal and backward transmission of error. The input layer receives the supplied input parameters during the forward transmission of the network signal, which are communicated to the implicit layer, which processes and sends them to the output layer. If the error between the output value of the network and the target value does not reach the set target error, the network transmits the error backward and continuously adjusts the network parameters such as weights and thresholds until the prediction error of the network reaches the set target error [13, 14]. The neural network structure shown in Fig. 1 is created. The input layer has six units: grinding depth, grinding wheel linear velocity, feed velocity, AE signal RMS value, AE signal ring count value, and FFT peak value. The output layer is one unit of surface roughness. The next step is to determine the number of layers and the number of neurons in the hidden layer.

Among them, in the entire BP neural network training or prediction process, the hidden layer output value H can be calculated using Eq. 1.

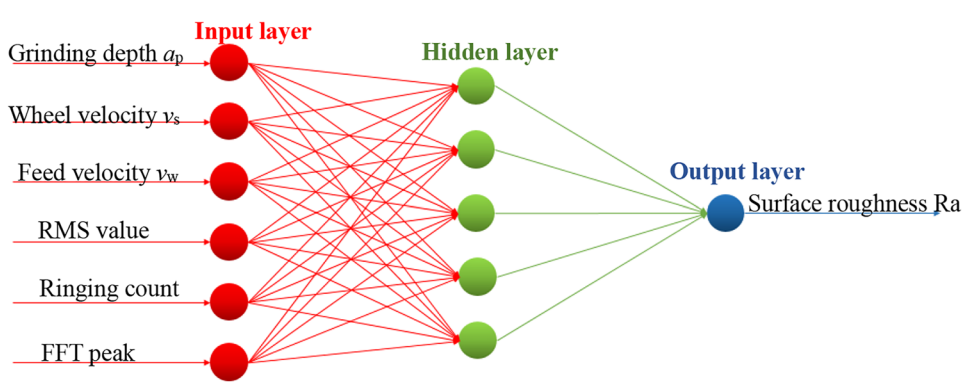

Fig. 1 Topological structure of BP neural network

$$H_j = f_1\left(\sum_{i=1}^{n} \omega_{ij} x_i - a_j\right) \tag{1}$$

According to the determination of the number of neurons in the hidden layer, in the prediction model of this paper, a total of five hidden layer output values are *H1–H5* conducted backward after each calculation. After calculating H, the output value O is further calculated from Eq. 2.

$$O_k = f_2\left(\sum_{j=1}^{l} H_j \omega_{jk} - b_k\right) \tag{2}$$

In the prediction model of this paper, there is only one output value O. Then the output value O is compared with the target output value.

Here, the hidden layers and the number of their neurons are determined based on the experimentally obtained data.

The hidden layers of BP neural networks can be divided into single hidden layers and multiple hidden layers according to the number of layers. It is generally believed that the network with multiple hidden layers has stronger prediction ability and can effectively reduce the network error, but the increase in the number of hidden layers will not only make the network more complex, but also increase the training time of the network. Therefore, when building the model, the BP neural network with a single hidden layer should be preferred, and a lower network training error can be obtained by setting the number of neurons in the hidden layer. Therefore, the number of hidden layers of the prediction model is determined as 1.

The number of neurons in the hidden layer should not be too few or too many. Because the number of neurons is too small, the network cannot be adequately trained; it is difficult to establish complex mapping relationships, and the training accuracy and prediction accuracy will be correspondingly large; too many neurons, the training time of the network will increase, but it will make the network generalization ability decrease and the prediction error increase. The number of neurons in the hidden layer can be determined by Eq. (3) [15].

$$l = \sqrt{m+n} + a \tag{3}$$

where l is the number of neurons in the hidden layer; m is the number of neurons in the output layer, n is the number of neurons in the input layer, and a is the modulation constant between 1 ~ 10.

The number of neurons in the hidden layer is chosen by first using the formula to estimate the approximate range of the number of neurons, and then choose the least number of neurons possible. The number of neurons in the hidden layer of the prediction model is initially determined as 4, 5, 6, and 7, and then the models containing different numbers of neurons in the hidden layer are trained separately, and the optimal number of neurons in the hidden layer is determined by comparing the training error size of the networks.

The surface roughness prediction model was trained with samples from the three material grinding experiments in Sect. 2, using 4, 5, 6, and 7 numbers of implied layer neurons respectively. The training error curves obtained after training are shown in Fig. 2, and the regression analyses obtained are shown in Fig. 3.

In can be seen from Fig. 2, during the training process, the mean square error (MSE) between the output value and the target value of the network reach the target error of 10^{-5} only when the number of neurons in the hidden layer is 5, while when the number of neurons in the hidden layer is 4, 6, and 7, the network does not reach the target training error before training stops, because the maximum number of failures of the network validation check has exceeded the set number of 10 times. That is, the error between the output value of the network and the target value no longer decreases during these 10 checks, and in order to prevent overfitting, the network has stopped training before reaching the target error.

The curves in the figure also show that the ideal mean square error in the network validation check reaches roughly 10^{-4}, and the network performance is pretty high only when the number of neurons in the hidden layer is 5. In addition, it can be seen from the regression analysis plot in Fig. 3 that the output value of the network is closest to the target value only when the number of neurons in the hidden layer is 5. The correlation coefficient $R = 0.9999$ and $R = 1$ indicates that the output value of the network is exactly equal to the target value, and in summary, the training accuracy of the network is highest when the number of neurons in the hidden layer is 5. The number of hidden layers in Fig. 1 is 5. Thus the topological structure of surface roughness in this paper is determined.

3 Grinding experiment

The grinding experiments were completed on a 2M9120 tool grinder, and the surface roughness of the ground workpiece was measured by a Micromeasure 3D profiler. The AE signal acquisition system includes PXDAQ12204 standard data acquisition card produced by Pengxiang Technology, AE144S, resonant high-sensitivity acoustic emission sensor produced by Fuji Co., Ltd. and PXPA III low-frequency acoustic emission preamplifier produced by Pengxiang Technology. The experimental system is shown in Fig. 4. The width of the workpiece used in the experiment is 18 mm. The grinding wheels used in the experiment are vitrified bond and resin bond grinding wheels. The specifications of the two grinding wheels are as follows: particle size 120#;

Fig. 2 Training error curve. **a** 4 hidden layer neurons, **b** 5 hidden layer neurons, **c** 6 hidden layer neurons, **d** 7 hidden layer neurons

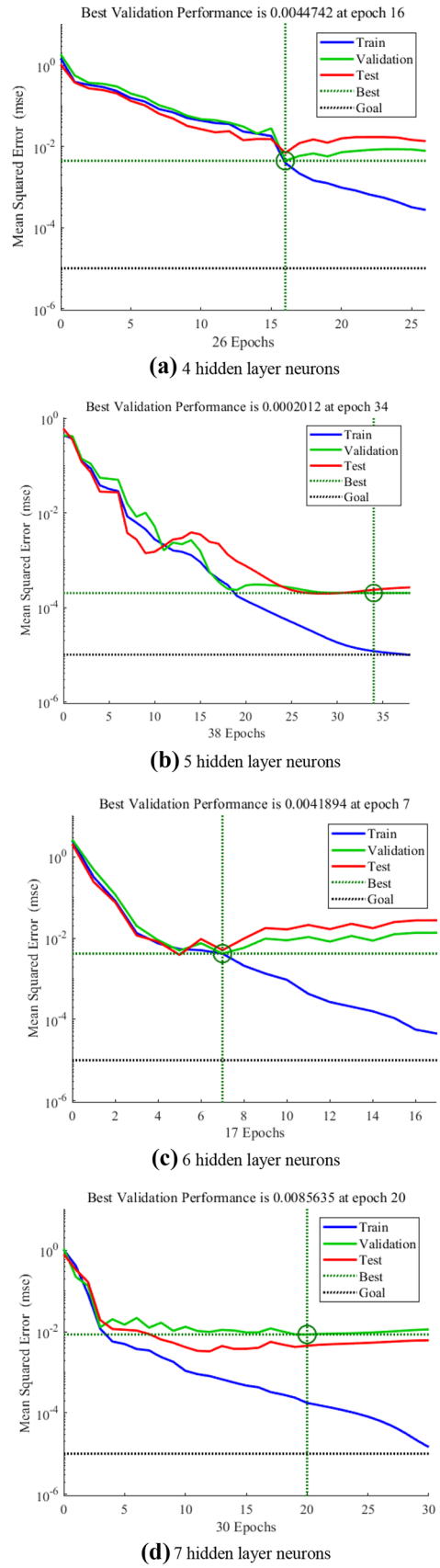

concentration 100%; abrasive layer width and thickness 5 mm; grinding wheel diameter 180 mm; inner hole diameter 32 mm.

Resin bond CBN grinding wheel and vitrified bond CBN grinding wheel were used to grind GH4169 superalloy, TC4 titanium alloy, and SiCp/Al composite materials. In order to study the changes of AE signals caused by the changes of individual factors during the grinding of difficult-to-machine alloys, the single-factor experimental research method was used to study the effects of grinding process parameters, workpiece materials, and wheel types on the AE signals. The experimental parameters are shown in Table 1.

4 Result and discussion

4.1 Effect of grinding parameters on AE signal characteristic parameters

4.1.1 Effect of grinding depth ap on AE signal characteristic parameters

As shown in Fig. 5, the AE signal RMS value increases with the increase of a_p when grinding workpieces of the above three materials. Because the volume of material removed during each grinding increases as the grinding depth increases, while the feed velocity and the outer contour size of the workpiece remain constant, the unit material removal rate increases, the deformation of grinding chips increases, and more energy is released, and the AE signal RMS value tends to rise. In addition, increasing the grinding depth will increase the contact area between the grinding wheel and the workpiece, increase the grinding force and enhance the interaction between the grinding wheel and the workpiece, which also has an increasing effect on the AE signal RMS value.

The AE signal RMS values corresponding to the grinding of the three materials with the same grinding wheel under the same grinding conditions are likewise considerably varied, as can be seen in the figure. Because when grinding TC4 titanium alloy, the temperature of the grinding zone is higher than when grinding GH4169 superalloy, and there are a lot of sparks splashing when grinding TC4 titanium alloy, which causes more energy to be released; the AE signal RMS value corresponding to grinding TC4 titanium alloy is significantly higher than that corresponding to grinding GH4169 superalloy; when grinding the SiCp/Al composite material, the SiC particles will release a large amount of energy due to the crushing of the SiC particles, so the RMS value of the AE signal is very large. In addition,

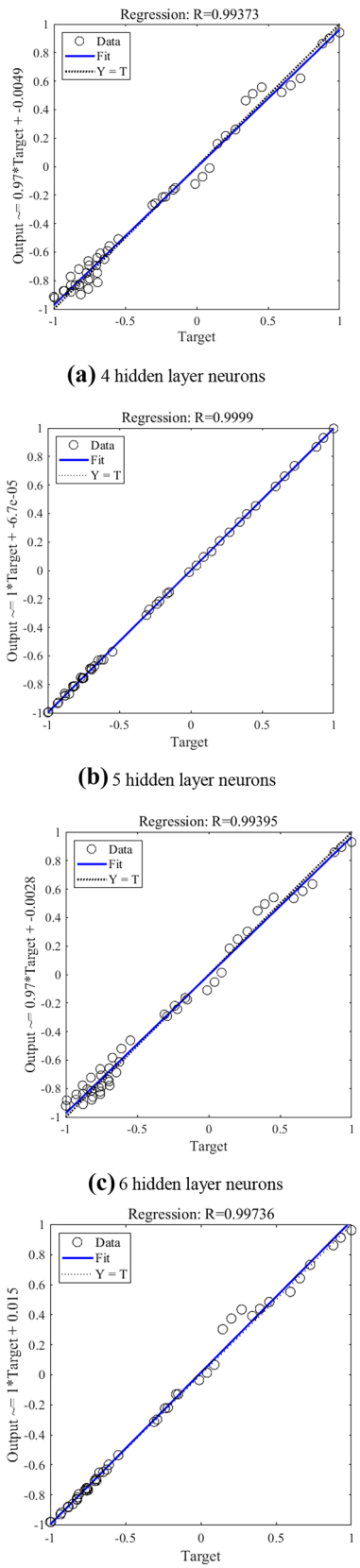

(a) 4 hidden layer neurons

(b) 5 hidden layer neurons

(c) 6 hidden layer neurons

(d) 7 hidden layer neurons

◀**Fig. 3** Regression diagram. **a** 4 hidden layer neurons, **b** 5 hidden layer neurons, **c** 6 hidden layer neurons, **d** 7 hidden layer neurons

when grinding the same material with the same grinding parameters, the AE signal RMS value corresponding to resin bonded CBN grinding wheel is larger than that corresponding to vitrified bonded CBN grinding wheel; this is because the resin grinding wheel creates larger grinding force, the interaction between the abrasive grain and the material is stronger, and the plastic deformation of the material is larger, so the RMS value of the corresponding AE signal is greater.

As shown in Fig. 6, the AE signal ringing count value increases with the increase of a_p when grinding workpieces of the above three materials. This is because with the increase of grinding depth, the contact area of single abrasive grain with the material increases, the extrusion contact with the material is strong, the material removal is obvious, and the AE signal generated is enhanced, which leads to the increase of the AE signal ringing count value. In addition, increasing the grinding depth will cause more abrasive grains on the grinding wheel surface to participate in grinding, resulting in more contact, scratching, and collision between the abrasive grains and the material, which will lead to an increase in the ringing count.

The figure also shows that at the same grinding conditions, the magnitude of the AE signal ringing count value corresponding to the three materials with the same type of grinding wheel varies slightly. Because the wear resistance of TC4 titanium alloy is not as good as that of GH4169 superalloy, and the elastic deflection of titanium alloy during grinding is smaller, so the material removal of TC4 titanium alloy is larger than that of GH4169 superalloy in

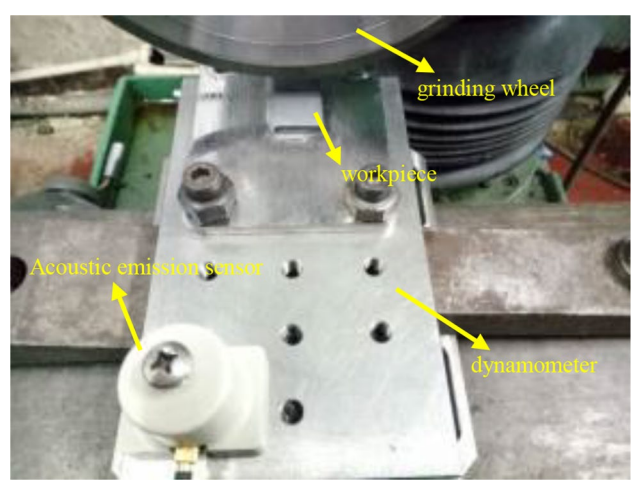

Fig. 4 Experimental system

Table 1 Single factor experimental parameters

Number	a_p (μm)	v_s (m/s)	v_w (m/min)
1	20/30/40/50	25	0.75
2	30	20/30/35	0.75
3	30	25	0.6/0.9/1.05

one grinding process, which will make more abrasive grains interact with the material, resulting in larger corresponding AE signal ringing count value. When grinding the SiCp/Al composite material, a large amount of aluminum matrix adheres to the surface of the grinding wheel, which reduces the number of abrasive particles involved in the grinding, which leads to the reduction of the corresponding AE signal ringing count value during grinding. In addition, when grinding the same material with the same grinding parameters, the AE signal ringing count value for resin bonded CBN wheel grinding is larger than that for vitrified bonded CBN wheel grinding; this is because, compared with resin grinding wheels, the adhesion of the material on the surface of the grinding wheel is more serious when the vitrified bond grinding wheel is grinding, which makes the number of abrasive grains involved in grinding relatively small, which in turn leads to a relatively small value of the AE signal ringing count.

4.1.2 Effect of grinding wheel linear velocity vs on AE signal characteristic parameters

As shown in Fig. 7, when grinding workpieces of the above three materials, the RMS value of the AE signal decreases with the increase of v_s. With the increase of the grinding wheel linear velocity, the number of abrasive grains passing through the grinding zone per unit time increases, the maximum undeformed chip thickness of a single abrasive grain decreases, the strain rate of the material decreases, the grinding force on a single abrasive grain decreases, the scratches on the workpiece surface are relatively shallow, and the material is removed without sufficient plastic deflection. The smaller the strain rate and plastic deflection of the material in the grinding process, the less energy will be released and the smaller the AE signal RMS value. Comparing the AE signal RMS values corresponding to the same grinding wheel grinding different materials under the same

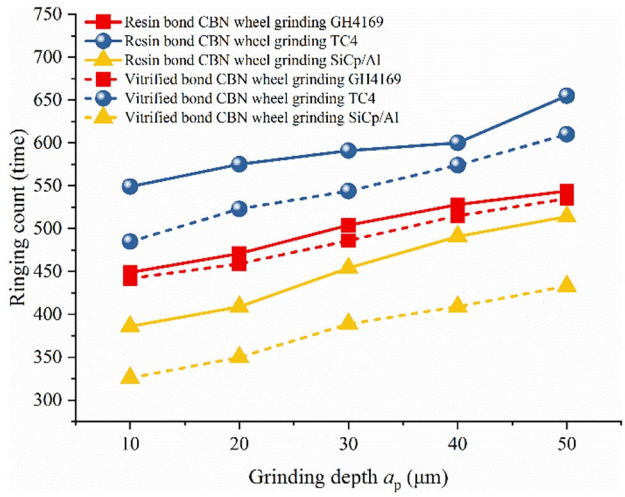

Fig. 6 Effects of grinding depth on the ringing count value of AE signal

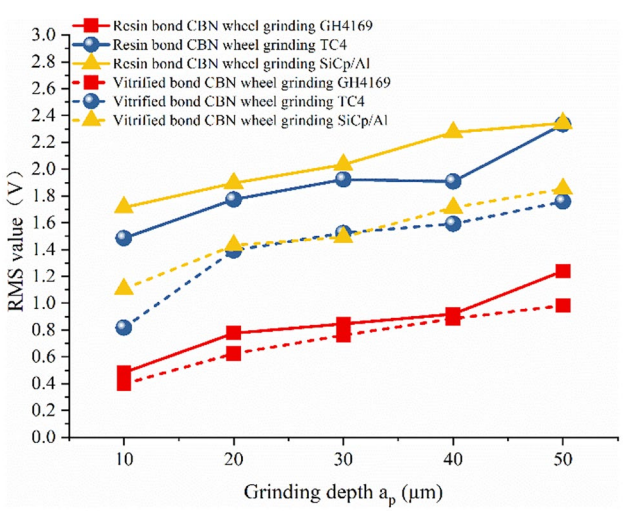

Fig. 5 Effects of grinding depth on the RMS value of AE signal

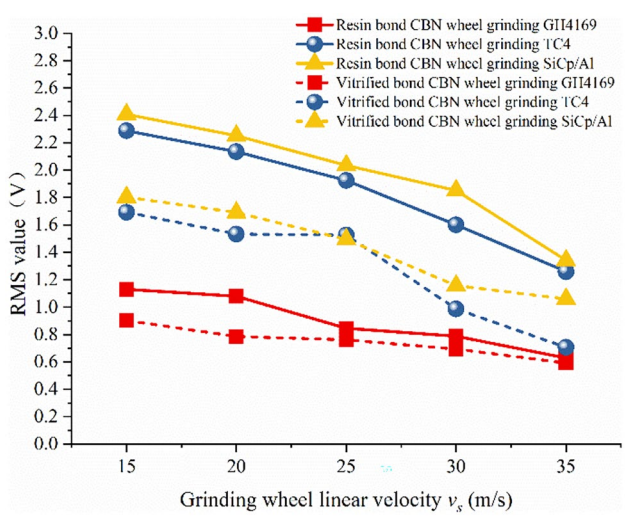

Fig. 7 Effects of the linear velocity of grinding wheel on the RMS value of AE signal

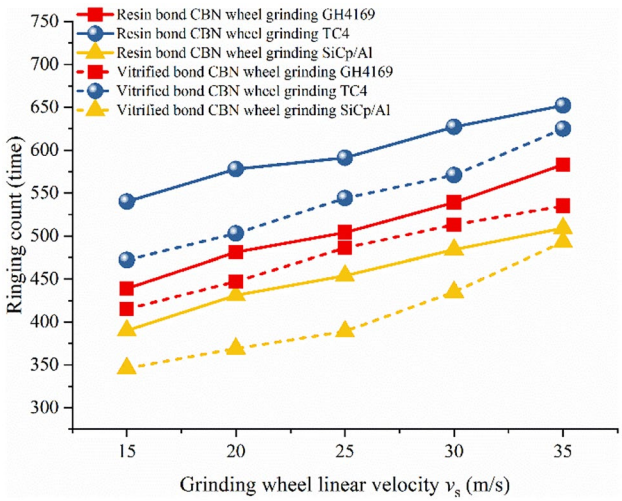

Fig. 8 Effects of the linear velocity of grinding wheel on the ringing count value of AE signal

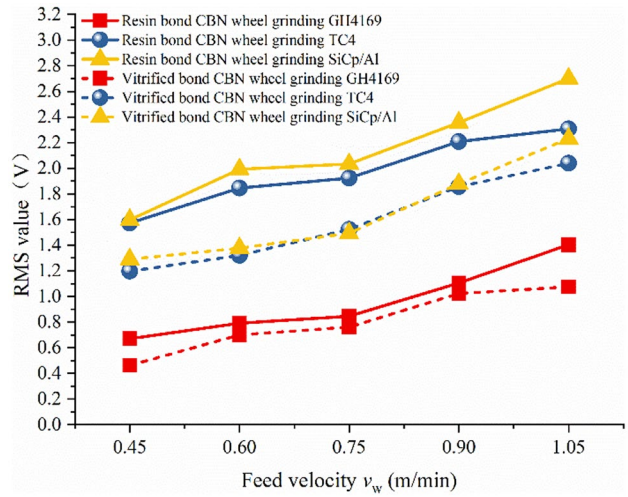

Fig. 9 Effects of feed velocity on the RMS value of AE signal

grinding parameters and different grinding wheels grinding the same material under the same grinding parameters, the same conclusion as before can be obtained and will not be repeated here.

As shown in Fig. 8, when grinding workpieces of the above three materials, the overall trend of the AE signal ringing count value increases with the increase of v_s. This is because as the grinding wheel linear velocity increases, the number of abrasive grains involved in grinding per unit time in the grinding zone increases, and the number of collisions and scratches between the abrasive grains and the material increases, so the AE signal ringing count value increases. Comparing the AE signal ringing count values corresponding to the same grinding wheel grinding different materials under the same grinding parameters and different grinding wheels grinding the same material under the same grinding parameters, the same conclusions as before can be obtained and will not be repeated here.

4.1.3 Effect of feed velocity vw on AE signal characteristic parameters

When grinding workpieces of the above three materials, the RMS value of the AE signal increases with the increase of v_w, as shown in Fig. 9. This is because as the feed velocity increases, the arc length of contact between a single abrasive grain and the material increases, and the undeformed chip thickness of the material increases, resulting in an increase in grinding force. In addition, the energy released during grinding is proportional to the strain rate of the material. As the feed velocity increases, the unit workpiece material removal increases, and the material strain rate increases, so the RMS value of the AE signal also increases. Comparing the corresponding AE signal RMS values when grinding different materials with the same grinding wheel at the same grinding parameters and when grinding the same material with different grinding wheels at the same grinding parameters, the same conclusions as before can be obtained and will not be repeated here.

As shown in Fig. 10, the AE signal ringing count value increases with the increase of v_w when grinding the above three materials; with the increase of feed velocity, the amount of material removal per unit time increases, the material removal becomes more and more obvious, and the AE signal is gradually enhanced, so the AE signal ringing count value shows a trend of gradual increase. Comparing the AE signal ringing count values when grinding different materials with

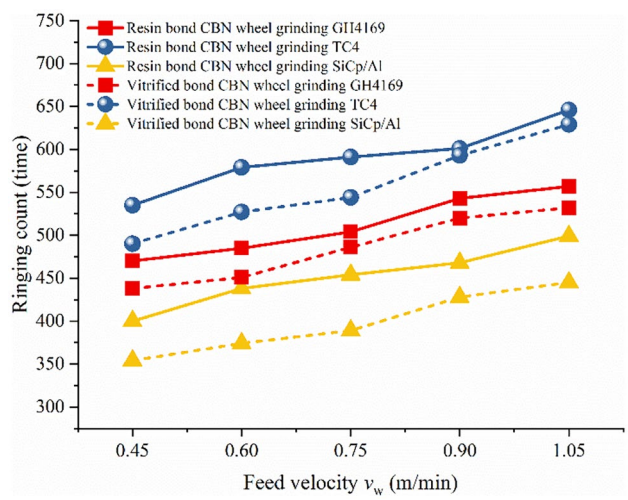

Fig. 10 Effects of feed velocity on the ringing count value of AE signal

the same grinding wheel at the same grinding parameters and when grinding the same material with different grinding wheels at the same grinding parameters, the same conclusion as before can be obtained and will not be repeated here.

4.2 Spectrum analysis of the grinding AE signal

In the grinding process, when grinding the same material with the same kind of grinding wheel, the changes of grinding parameters will lead to certain changes in the AE signal spectrum. Taking the grinding of GH4169 superalloy with resin-bonded CBN grinding wheel as an example, the effects of each grinding parameter on the AE signal spectrum were analyzed, and it was found that the peaks of the main energy concentration bands of the AE signal spectrum corresponding to different grinding parameters differed greatly, as shown in Figs. 11, 12, 13.

As shown in Fig. 11, the spectral energy corresponding to GH4169 grinding at various grinding depths is mainly distributed between 90 and 140 kHz, with the spectral amplitude of other frequency bands being very small, and the spectral amplitude of this band increasing gradually as the grinding depth increases, because the spectral amplitude represents the magnitude of the energy released during the grinding process. The greater the grinding depth, the more energy is released in the grinding process, so the spectrum amplitude is larger, which is consistent with the trend of the AE signal RMS with the grinding depth analyzed earlier.

As can be seen from Fig. 12, with the increase of the grinding wheel linear velocity, the spectral amplitude of the main energy concentration band between 90 and 140 kHz gradually decreases, which is because with the increase of the grinding wheel linear velocity, the strain rate and plastic deflection of the material decreases, and the energy released decreases, so the corresponding spectral amplitude gradually decreases, which is consistent with the trend of the RMS value of the AE signal with the grinding wheel line velocity analyzed earlier.

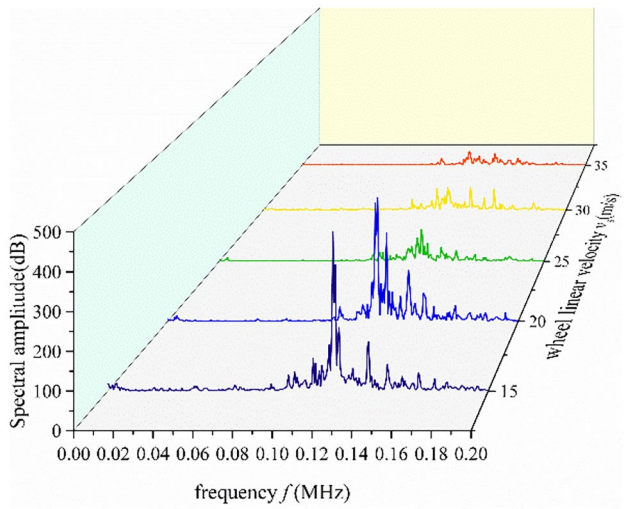

Fig. 12 Effects of the linear velocity of grinding wheel on the spectrum of AE signal

As can be seen from Fig. 13, with the increase of the feeding velocity, the spectral amplitude of the main energy concentration band between 90 and 140 kHz is gradually increasing, which is because with the increase of the feeding velocity, the amount of material removal per unit time increases, the strain rate of the material increases, and the energy released increases, so the spectral amplitude gradually increases, which is consistent with the trend of the RMS value of the AE signal with the feeding velocity analyzed earlier.

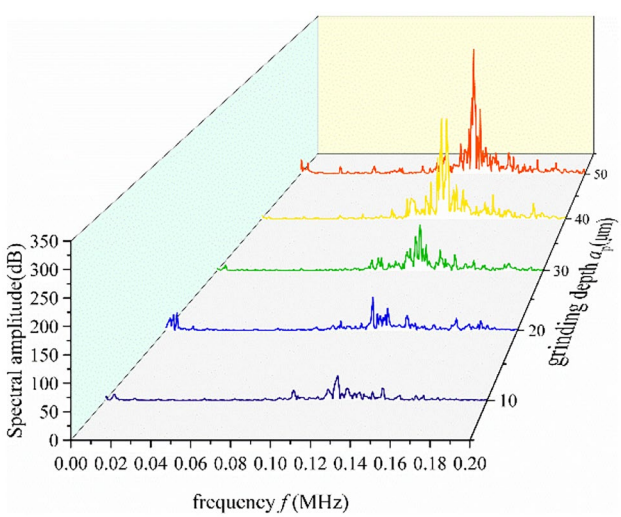

Fig. 11 Effects of grinding depth on the spectrum of AE signal

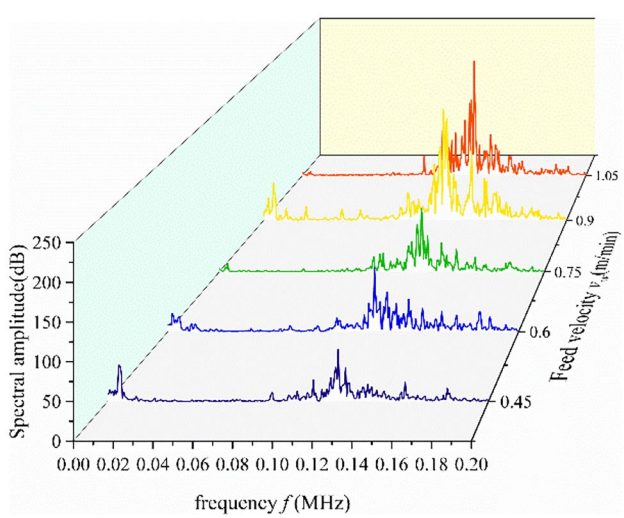

Fig. 13 Effects of feed velocity on the spectrum of AE signal

Fig. 14 The relationship between surface roughness and characteristic parameters of AE signal. **a** The relationship between R_a and RMS value. **b** The relationship between R_a and ringing count. **c** The relationship between R_a and FFT peak

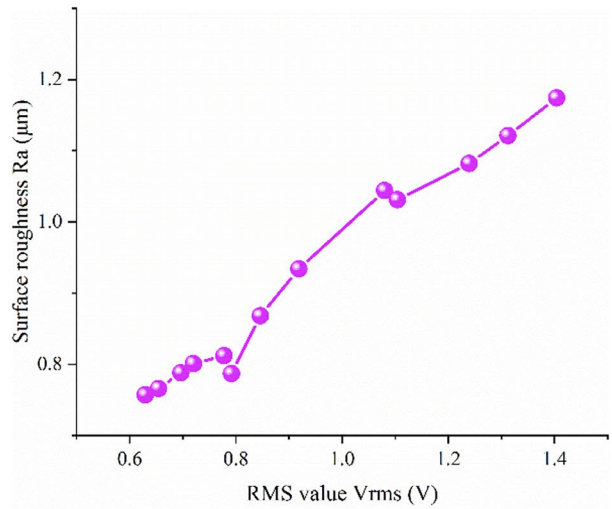

(a) The relationship between R_a and RMS value

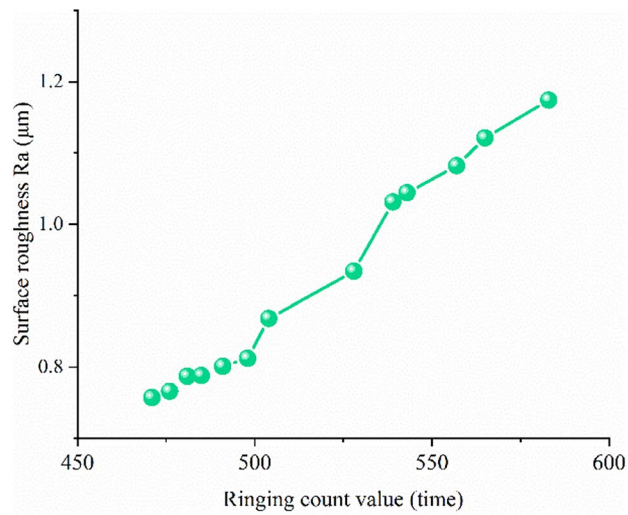

(b) The relationship between R_a and ringing count

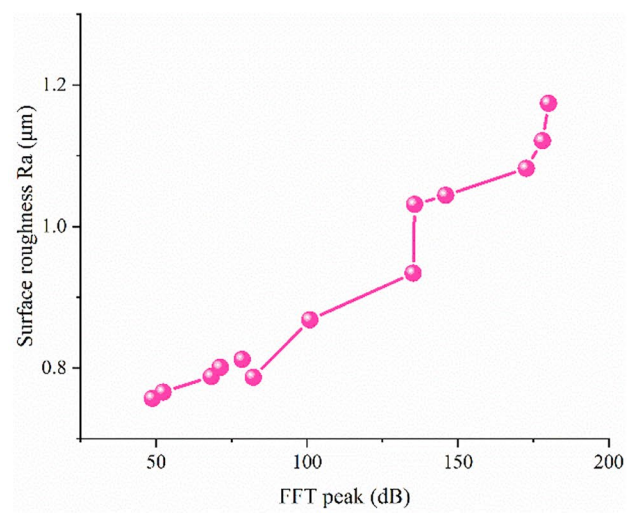

(c) The relationship between R_a and FFT peak

4.3 Study on the relationship between grinding surface roughness and AE signal characteristics

This section will investigate the relationship between the RMS value, ringing count, FFT peak, and surface roughness of the acoustic emission signal in order to improve the prediction reliability of the succeeding surface roughness prediction model and offer trustworthy input parameters.

The resin bond CBN grinding wheel was used to grind a set of processing parameters in the GH4169 superalloy, i.e., 13 times, and 13 sets of acoustic emission signals were collected to obtain the acoustic emission signal characteristic parameters corresponding to each set of experiments, and the FFT transform of the acoustic emission time-domain waveform was performed to obtain the FFT peak corresponding to each set of experiments, and the surface roughness was measured to obtain the relationship between the grinding surface roughness and the acoustic emission signal, and the corresponding relationship between the surface roughness and the acoustic emission signal was obtained. The results of the experiments are shown in Fig. 14.

It can be observed in Fig. 14a that the surface roughness values of the workpiece corresponding to different RMS values of acoustic emission signals during the grinding process are different, and the larger the RMS value is, the larger the surface roughness value is; it can be found in Fig. 14b that the workpiece surface roughness values corresponding to different acoustic emission signal ringing count values are different, and from the overall trend, the larger the acoustic emission signal ringing count value is, the larger the corresponding surface roughness value is; it can be found in Fig. 14c that the workpiece surface roughness values corresponding to different FFT peaks are different, and the larger the FFT peak value is, the larger the corresponding surface roughness value is. The RMS value of the acoustic emission signal, the ringing count value, the FFT peak value, and the grinding surface roughness value all have a high correlation and may be utilized as input parameters for the future grinding surface roughness multi-information fusion prediction model.

5 Modeling surface roughness prediction

Some training parameters must be established before the BP neural network can begin training in order for the network to get better prediction outcomes. The main training parameters for this prediction model are set as follows:

Set the training times of the network to 100; set the learning rate of the network, which should be taken as 0.05 between

[0, 1]; set the target minimum error of the network, which is the mean square error between the predicted and expected values of the network after each training, and here it is set to 0.00001; set the maximum number of failures of the network validation check to 10.

The training sample data obtained from the experiments were used to train the prediction model shown in Fig. 1, and after training, the grinding surface roughness R_a was predicted, and the surface roughness values predicted by the network were compared with those obtained from the experiments, as shown in Fig. 15.

The gap between the anticipated and experimental surface roughness values was not substantial, and the change trend was the same, according to the surface roughness values of each sample corresponding to two locations in the figure. Based on the absolute error between the predicted and experimental values, a regression analysis was performed on the two sets of values, as shown in Fig. 16. The horizontal axis indicates the surface roughness value obtained from the experiment, and the vertical axis indicates the predictive value of the network, and the size of the absolute error is indicated by different colors; if the points in the figure fall on the diagonal, it means that the predicted value is almost equal to the experimental value, and the color of the points is dark green; the farther away from the diagonal, it means that the absolute error between the predicted value and the experimental value is larger, and the color of the points with relatively large errors is dark red. The blue line in the figure is the fitted line after linear regression for all the points in the figure, and it can be seen that the line deviates from the diagonal line to some extent, but not much, and the correlation coefficient $R = 0.98742$ indicates that the absolute error between the predicted and experimental values of the network is not large.

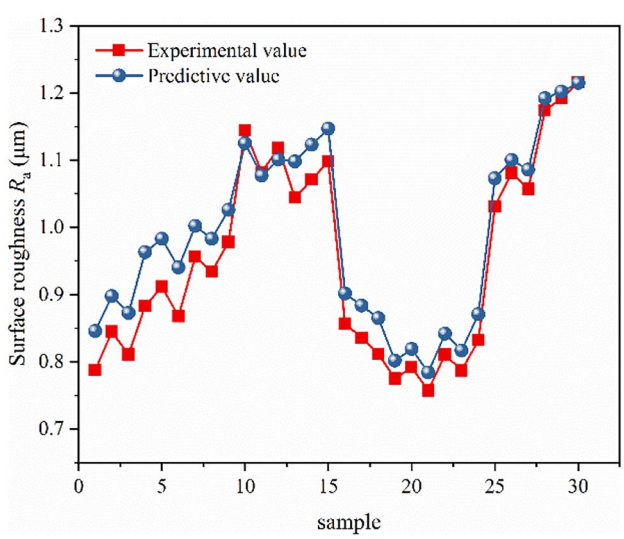

Fig. 15 Comparison diagram of predictive and experimental value

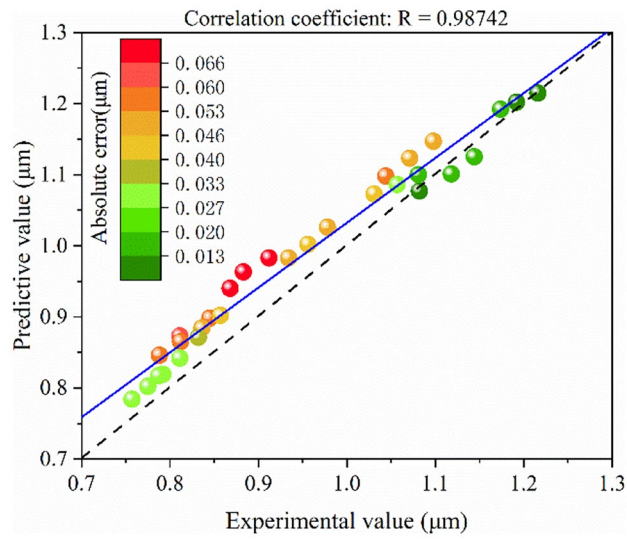

Fig. 16 The regression analysis diagram of the predictive and experimental value

Figure 17 shows the relative error curve between the predicted and experimental values of the network, and it can be seen that the relative error between all the predicted and experimental values is below 10%, among which the maximum relative error is 9.06% and the minimum relative error is 0.08%. In general, the prediction model's prediction accuracy is high, and it can achieve a certain prediction effect; however, there is still a large gap between the network prediction and the experimental value, so the model will be optimized using a genetic algorithm to obtain a more accurate prediction value.

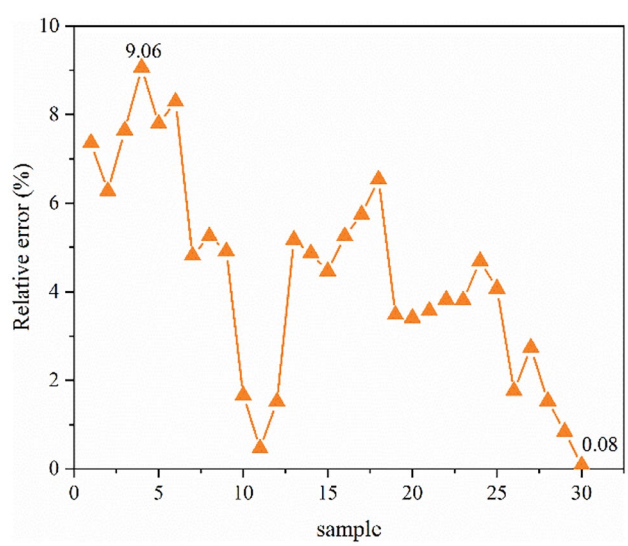

Fig. 17 The relative error between the predictive value and the experimental value

6 Model improvement and optimization using genetic algorithm

According to the study in subsection 4, despite the BP neural network prediction model's excellent prediction accuracy, there is still a considerable error between the network prediction value and the experimental value, necessitating BP neural network algorithm optimization to increase prediction accuracy. At present, the widely used optimization algorithm is genetic algorithm (GA), and the main purpose of applying genetic algorithm to optimize BP neural network is to obtain better initial weights and thresholds of the network through genetic operations.

In this process, the initialization parameters are set as follows: population size = 30; maximum evolutionary generations = 20; crossover probability = 0.3; and variation probability = 0.1. After setting the initialization parameters, we need to apply the coding function to each individual in the population, and then use the fitness function to calculate the fitness value of each individual, and find out the smallest fitness value and its corresponding optimal individual, and the initialization operation of the genetic algorithm is completed. Although the optimal individuals in the initialized population have been identified, there may be more excellent individuals in the new population obtained after the genetic operation, so it is necessary to apply the selection function, crossover function, and variation function to select; crossover and mutate the individuals in the population, so that the population can be evolved for 20 generations; after the evolution is completed, the optimal individual is used as the initial weights and thresholds of the BP neural network prediction model, and the previous experimental data is also used for training, and then the data is predicted to obtain the predicted value of the optimized surface roughness.

Figure 18 shows the change curve of the optimal individual fitness value; it can be seen from the figure that during the evolution of the population, the optimal individual fitness value decreases rapidly and stops decreasing after reaching the minimum value, which indicates that the error between the network output value and the target value decreases rapidly with the evolution of the population, and when the number of evolution reaches the maximum number of evolutionary generations, the evolution stops and the optimal individual is obtained, i.e., the optimal network initial weight and threshold value.

Compare the predicted value of the network before and after the optimization with the experimental value, as shown in Fig. 19. Observing the surface roughness values corresponding to the same sample in the figure, it is found that the predicted values of the network optimized by the genetic algorithm are closer to the experimental values, indicating that the individuals obtained after 20 evolutions are excellent and can make the predictions more reliable.

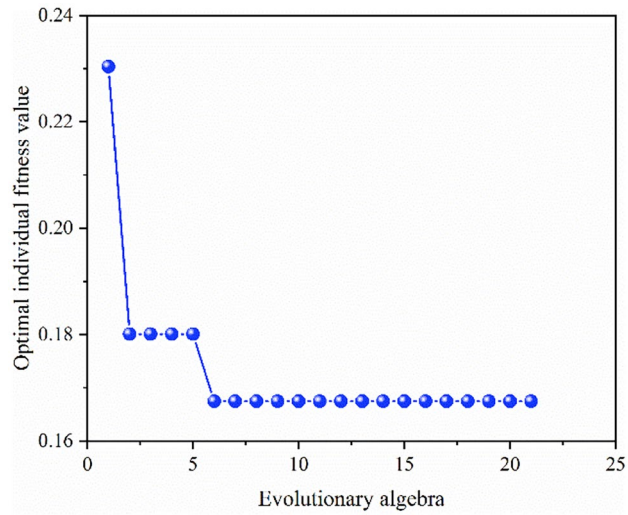

Fig. 18 The optimal individual fitness value

Figures 16, 20 show the regression analysis diagrams of the prediction errors of the network before and after optimization, respectively. Comparing the two figures, it can be found that the linear regression fitting line between the predicted and experimental values after optimization is closer to the diagonal line; the color of most points in the figure is green, and the correlation coefficient $R = 0.99558$, which is larger than that before optimization. As a result, the absolute error between the genetic algorithm's network prediction value and the experimental value is less and closer to the experimental value. The accuracy of the prediction is better.

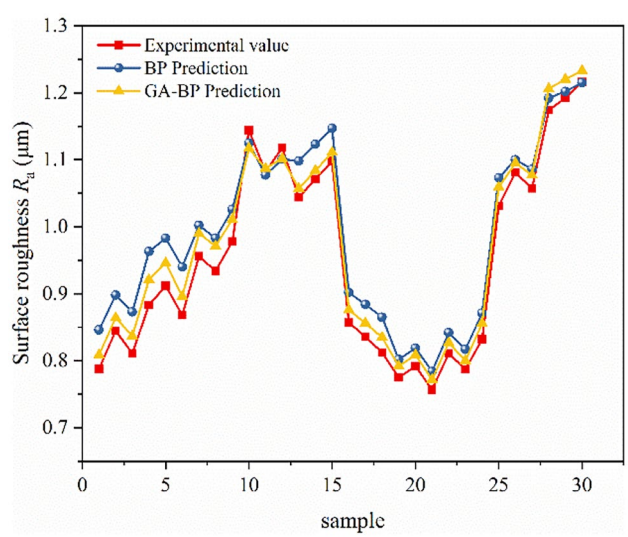

Fig. 19 Comparison of the predicted and experimental values before and after optimization

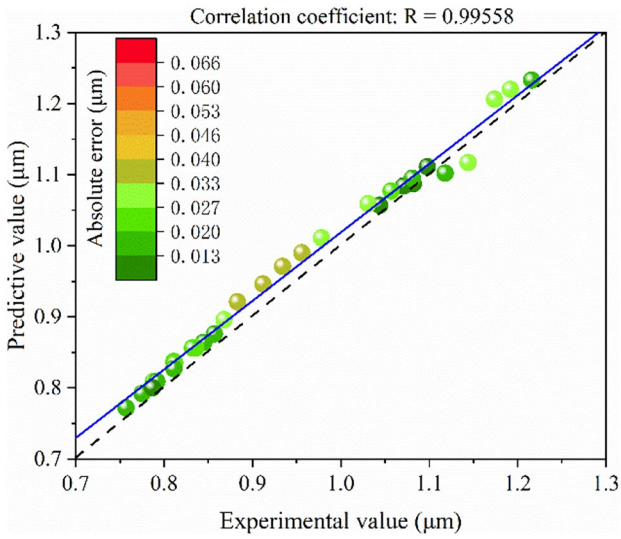

Fig. 20 The regression analysis diagram before and after optimization

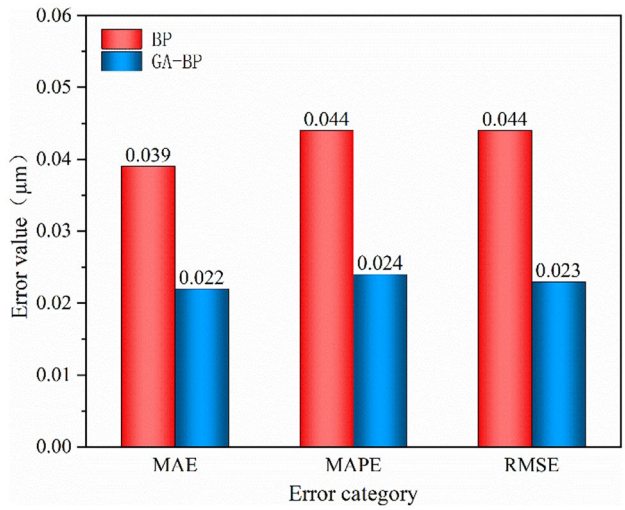

Fig. 22 Error comparison histogram

Figure 21 shows the comparison diagram of the relative error between the network predicted value and the experimental value before and after optimization. Comparing the relative errors corresponding to the same sample in the figure, it is found that the relative errors of the predicted values of the BP neural network optimized by the genetic algorithm are smaller. The relative errors of all samples before optimization were below 10%, and the relative errors of all samples after optimization were reduced to below 5%, where the maximum relative error was 4.30% and the minimum relative error was 0.46%; on the whole, the error of the predicted values after optimization relative to the experimental value is smaller.

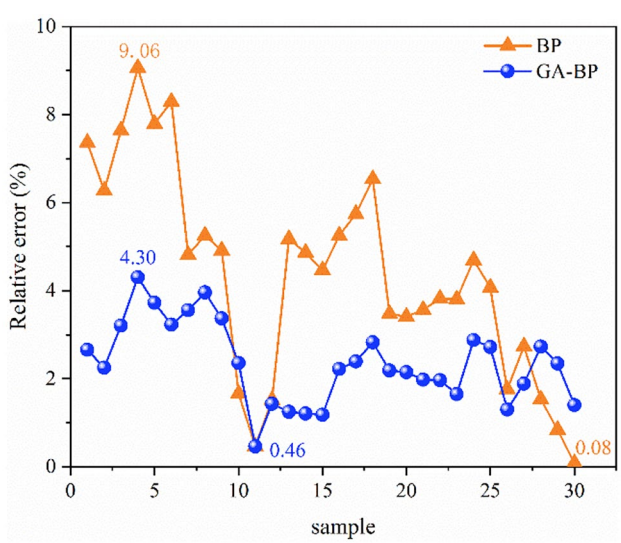

Fig. 21 Comparison of relative errors before and after optimization

Figure 22 shows the comparison histogram of the size of each error in the predicted values of the network before and after optimization. The compared errors are mean absolute error (MAE), mean absolute percent error (MAPE), and root mean square error (RMSE); since the value of MAPE displayed as a percentage is relatively large, the histogram display of the other two errors is not obvious, and the value of MAPE is converted to a decimal display. Overall, the reduction in each error of the predicted values after optimization by the evolutionary algorithm is extremely noticeable, indicating that the optimized network's prediction performance is superior to the pre-optimized network.

7 Conclusions

In this paper, a combination of theory and experiment has been conducted to investigate the surface roughness prediction model based on BP neural network; the following conclusions can be drawn.

(1) The RMS value of the AE signal increased with the increase of grinding depth a_p and feed velocity v_w, and decreased with the increase of grinding wheel linear velocity v_s, when grinding GH4169 superalloy, TC4 titanium alloy, and SiCp/Al composite; the ringing count value increased with the increase of a_p, v_s, and v_w. The RMS value corresponding to the grinding of SiCp/Al composite with the same grinding wheel was the highest, while the RMS value corresponding to the grinding of GH4169 superalloy was the lowest, under the same grinding settings; the ringing count value associated with TC4 titanium alloy grinding was the

highest, whereas the ringing count value associated with SiCp/Al composite grinding was the lowest. The RMS and ringing count values of the AE signal corresponding to the grinding of the resin bond CBN grinding wheel are larger than those of the vitrified bond CBN grinding wheel when grinding the same material with the same grinding parameters.

(2) A good match is identified between the AE signal RMS value, ringing count value, and FFT peak value and the grinding surface roughness by the analysis of the related relationship between the grinding surface roughness and the AE signal.

(3) Although the multi-information fusion model developed in this study can predict grinding surface roughness, there are several flaws. Following the development of the model using a genetic algorithm, it was discovered that the optimized model's surface roughness prediction accuracy and recognition accuracy of the grinding wheel wear condition had substantially improved.

Author contribution Guoqiang Yin: investigation, conceptualization, methodology, experiment, writing—original draft. Jiahui Wang: investigation, experiment, writing—reviewing and editing. Yunyun Guan: investigation, experiment. Dong Wang: funding. Yao Sun: funding, supervision.

Funding This work is supported by the National Natural Science Foundation of China (No. 51771193, 52005092) and the Fundamental Research Funds for the Central Universities (No. N2103013).

Data availability The datasets used or analyzed during the current study are available from the corresponding author on reasonable request.

Code availability Not applicable.

Declarations

Ethics approval The authors state that the present work is in compliance with the ethical standards.

Consent to participate All the authors consent to participate this work.

Consent for publication All authors agree to publish.

Competing interests The authors declare no competing interests.

References

1. Sun C, Xiu SC, Zhang P, Li QL, Zou XN, Ma L (2022) Influence of the dynamic disc grinding wheel displacement on surface generation. J Manuf Process 75:363–374
2. Li QL, Xiu SC, Sun C, Yao YL, Kong XN (2022) Analysis of the uniformity of material removal in double-sided grinding based on thermal–mechanical coupling. Int J Adv Manuf Technol 1–13
3. Hundt W, Leuenberger D, Rehsteiner F, Gygax P (1994) An approach to monitoring of the grinding process using acoustic emission (AE) technique. CIRP Ann Manuf Technol 43(1):295–298
4. Liu GJ, Gong YD, Wang WS (2001) Applications of acoustic emission technology in monitoring of grinding processes. Mech Eng 12:4–6
5. Sun Y, Jin LY, Gong YD, Wen XL, Yin GQ, Wen Q, Tang BJ (2022) Experimental evaluation of surface generation and force time-varying characteristics of curvilinear grooved micro end mills fabricated by EDM. J Manuf Process 73:799–814
6. Pan YH, Wang YH, Zhou P, Yan Y, Guo DM (2020) Activation functions selection for BP neural network model of ground surface roughness. J Intell Manuf 31(8)
7. Dornfeld D, Cai HG (1984) An investigation of grinding and wheel loading using acoustic emission. J Ind Eng Chem 106(1):28–33
8. Ding N, Zhao CL, Luo XC, Li QH, Shi YC (2017) An intelligent prediction of surface roughness on precision grinding. Solid State Phenom 261:221–225
9. Pandiyan V, Caesarendra W, Tjahjowidodo T, Tan HH (2018) In-process tool condition monitoring in compliant abrasive belt grinding process using support vector machine and genetic algorithm. J Manuf Process 31:199–213
10. Arun A, Rameshkumar K, Unnikrishnan D, Sumesh A (2018) Tool condition monitoring of cylindrical grinding process using acoustic emission sensor. Mater Today 5(5):11888–11899
11. Liu CW, Chen HC, Lin SC (2019) Acoustic emission monitoring system for hard polishing of sapphire wafer. Sens Mater 31(9):2681–2689
12. Hweju Z, Abou-El-Hossein K (2020) Surface roughness prediction based on acoustic emission signals in high-precision diamond turning of rapidly solidified optical aluminum grade (RSA443). Key Eng Mater 841:363–368
13. Liu H, Xu SH, Ge XM, Zahid MA (2019) Automatic sedimentary microfacies identification from logging curves based on deep process neural network. Cluster Comput 22(5)
14. Wang R, Jiang JC, Pan Y, Cao HY, Cui Y (2009) Prediction of impact sensitivity of nitro energetic compounds by neural network based on electrotopological-state indices. J Hazard Mater 166(1):155–186
15. Gao L, Li F, Huo PD, Li C, Xu J (2021) Accurate prediction of the extrusion forming bonding reliability for heterogeneous welded sheets based on GA-BP neural network. Int J Adv Manuf Technol (3)

Publisher's Note Springer Nature remains neutral with regard to jurisdictional claims in published maps and institutional affiliations.